FATIGUE BEHAVIOR OF FERRITIC STAINLESS STEELS USED IN EXHAUST SYSTEMS

Leonardo Barbosa Godefroid
REDEMAT-UFOP, Praça Tiradentes, 20, 35400-000 Ouro Preto – MG
leonardo@demet.em.ufop.br

Ricardo Augusto Faria
REDEMAT-UFOP, ACESITA S.A., Praça 1º de maio, 9, 35180-018 Timóteo - MG
rafaria@acesita.com.br

Luiz Cláudio Cândido
REDEMAT-UFOP, Praça Tiradentes, 20, 35400-000 Ouro Preto – MG
candido@em.ufop.br

Max Eduardo Pereira
UFOP, Praça Tiradentes, 20, 35400-000 Ouro Preto – MG
leonardo@demet.em.ufop.br

Abstract. In this research, the fatigue behavior of five ferritic stainless steels – 409A, 430E, 439A, 441A and F17T - used in the automotive industry has been studied. These steels are candidates for use in exhaust systems. The main difference of the steels is the content of Nb and Ti as alloy elements. Constant axial load amplitude fatigue tests were performed under a stress ratio of R = 0.1. Testing frequency was 30Hz. The experiments were performed in ambient air (approximately 25°C, R.H. = 60%). Results showed that the fatigue resistance of the 430E steel stabilized with Nb was superior to the other steels.

Keywords: Fatigue, Ferritic Stainless Steels, Stabilization, Exhaust Systems.

1. Introduction

Stainless steel has been used variously nowadays owing to its many superior properties such as formability, strength, and corrosion resistance (Hiramatsu, 2001; Keown & Pickering, 1984). History of stainless steels is just about 100 years, which means very short term in comparison with other steels and metals. In addition, it has been as short as approximately 50 years since stainless steels has begun to be manufactured commercially and used for materials of many types of applications.

Type AISI 304 and type AISI 430 are well known as the most popular stainless steels and presumably dominate more than half of all products of stainless steels. However, demands for stainless steel has grown markedly in this decade. Consequently, various types of stainless steels with significantly good properties have been developed and used for many applications.

In recent years, one of the applications for stainless steels has been markedly growing, that is, materials of an exhaust gas emission control system for vehicles has been changed from carbon steel to stainless steel. Ferritic stainless steels are good candidates for this application (Douthett, 1995, Schmitt, 2002). Containing 11-30 percent Cr, generally little or no Ni, with additions of Mo, Nb and Ti, and low C and N contents, these steels are frequently fully ferritic from room temperature to the melting point, and have good corrosion resistance, formability, and heat resistance. Figure 1 shows an exhaust system with traditional stainless steels used in some parts of this system (Kawasaki Steel, 2001).

There are a number of standard ferritic steels (the AISI 400 series) that contain varying additions of alloy elements. Of these additions, Nb and Ti are strong ferrite formers, and also remove C and N from solution as insoluble carbides and nitrides (stable precipitates)(Gordon and Bennekom, 1996). This further stabilizes the ferrite and also protects against sensitization; the removal of C and N as insoluble carbonitrides can also improve the ductility and impact resistance (Pickering, 1979).

Whereas 80% of failures in steel exhausts are attributable to corrosion, it is found that the remaining 20% are due to fatigue (Llewellyn, 1994). Having improved the corrosion performance very substantially, fatigue therefore becomes the predominant mode of failure in stainless steels. For example, street conditions, exhaust system weight effect, and others are responsible for carrying out cyclic loads at the exhaust system that can be more dangerous than corrosion alone.

Therefore to ensure that a stainless steel exhaust system does not undergo premature failure due to fatigue, careful considerations must be given to design details, standards of manufacture and structure-property relationships. Extensive road trials have shown that attention to these details can provide exhausts with excellent fatigue characteristics, thereby ensuring the long-term integrity of stainless steel systems.

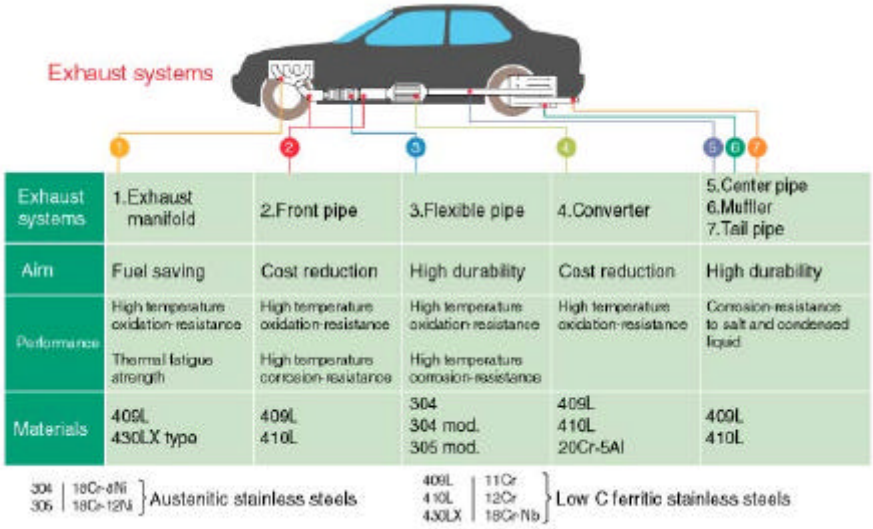

Figure 1. Schema showing an exhaust system for vehicles, and some materials candidates for this application.

The fatigue properties of stainless steels in air at room temperature show that the fatigue limit/tensile strength ratio is 0.3 : 0.5 for austenitic grades and 0.45 : 0.65 for duplex grades (for load ratios of R = -1). Austenitic stainless steels have higher fatigue strength/proof stress ratios than duplex stainless steels. It was also shown that there is a clear relationship between the fatigue limit and the ultimate tensile strength, but not between the fatigue limit and the proof stress (Bergengren et al., 1995). Fatigue data of ferritic stainless steels are not well known and must be evaluated.

In this research, the fatigue behavior of five ferritic stainless steels – 409A, 430E, 439A, 441A and F17T – candidates for use in exhaust system for vehicles has been studied. The main difference of the steels is the content of Nb and Ti as alloy elements. Constant axial load amplitude fatigue tests were performed and the results are analyzed in terms of S-N fatigue curves.

2. Materials and experimental procedure

2.1 Chemical composition and thickness

The chemical composition and thickness of the industrially produced steels used for this study are shown in Tab. 1. "P" denotes the fabrication of the steel in ACESITA S.A. (Brazil) while "F" denotes Ugine/ARCELOR (France). It's possible to see significant chemical differences between the steels.

Table 1. Chemical composition and thickness of the ferritic stainless steels grades (weight percent).

Steel	Cr	Ti	Nb	Mn	C + N (ppm)	ΔTi	ΔNb	Thickness (mm)
P409A	11.35	0.134	0.021	0.131	192	0.06	-------	1.535
P439A	17.05	0.196	0.194	0.120	235	0.14	0.14	1.556
P430E	16.23	0.011	0.356	0.239	399	-------	0.05	1.563
P441A	18.06	0.133	0.563	0.149	225	0.09	0.49	1.459
F17T	16.18	0.452	0.011	0.339	316	0.34	-------	1.408

ΔTi and ΔNb values represent the quantity of these elements in solid solution and is obtained by stoichometric equations. Depending of the kind of stabilization (Ti, Nb or Ti+Nb), there is a specific equation:

$\Delta Ti = Ti - 3{,}42\ N - 4\ C$ Ti stabilized grades (P409A and F17T)

$\Delta Nb = Nb - 7{,}74\ (C+N)$ Nb stabilized grades (P430E)

$\Delta Ti = Ti - 3{,}42\ N - (0{,}30 \times 4C)$ Duo stabilized grades (P439A and P441A)

$\Delta Nb = Nb - (0{,}70 \times 7{,}74C)$ Duo stabilized grades (P439A and P441A).

In Tab. 1, P409A grade is a 11%Cr alloy with Ti addition only; all the others alloys have a high chromium content (more than 16%), which P439A and P441A are duo stabilized grades, P430E grade is Nb stabilized while F17T grade is Ti stabilized. The aim of stabilization is to ensure ferrite stabilization from melting point to room temperature, what means, no other phase is expected.

2.2 Experimental procedures

Metallographic specimens in longitudinal and transversal directions were prepared and observed in an LEICA optical microscopy.

The tests conducted include monotonic tests in tension and fatigue tests, using smooth (unnotched) specimens. The specimens, Fig. 2, used in these tests were machined in the longitudinal direction, with continuous radius between ends, with a total length of 200 mm, and a rectangular cross section, as seen in ASTM E466-96.

Figure 2. Smooth specimen used in this research. Length = 200 mm; Width = 12.7 mm.

All mechanical tests were conducted under load control on a servo-controlled, hydraulically-actuated, closed-loop INSTRON mechanical test machine interfaced to a computer for machine control and data acquisition. The fatigue tests were performed at a frequency of 30 Hz, in ambient air (approximately 25°C, R.H. = 60%), at stress R-ratio of 0.1 (tension-tension cyclic loading). Fatigue tests were performed to measure the relation between the applied stress and the number of stress cycles to fracture (S-N curves) and to estimate the fatigue limit. Fracture surfaces were analyzed in a JEOL scanning electron microscope.

3. Results and discussion

3.1 Microstructure analysis

The microstructures of the five stainless steels studied in the transversal direction are presented in Fig. 3(a,b,c,d,e). Similar results are obtained in the longitudinal direction, indicating that it was not noticeable any major tendency for anisotropy.

The microstructure for all the studied grades was homogeneous and constituted of recrystallized grains. Table 2 presents the average grain size of the five ferritic stainless steels grades. The measurement was done in the rolling direction.

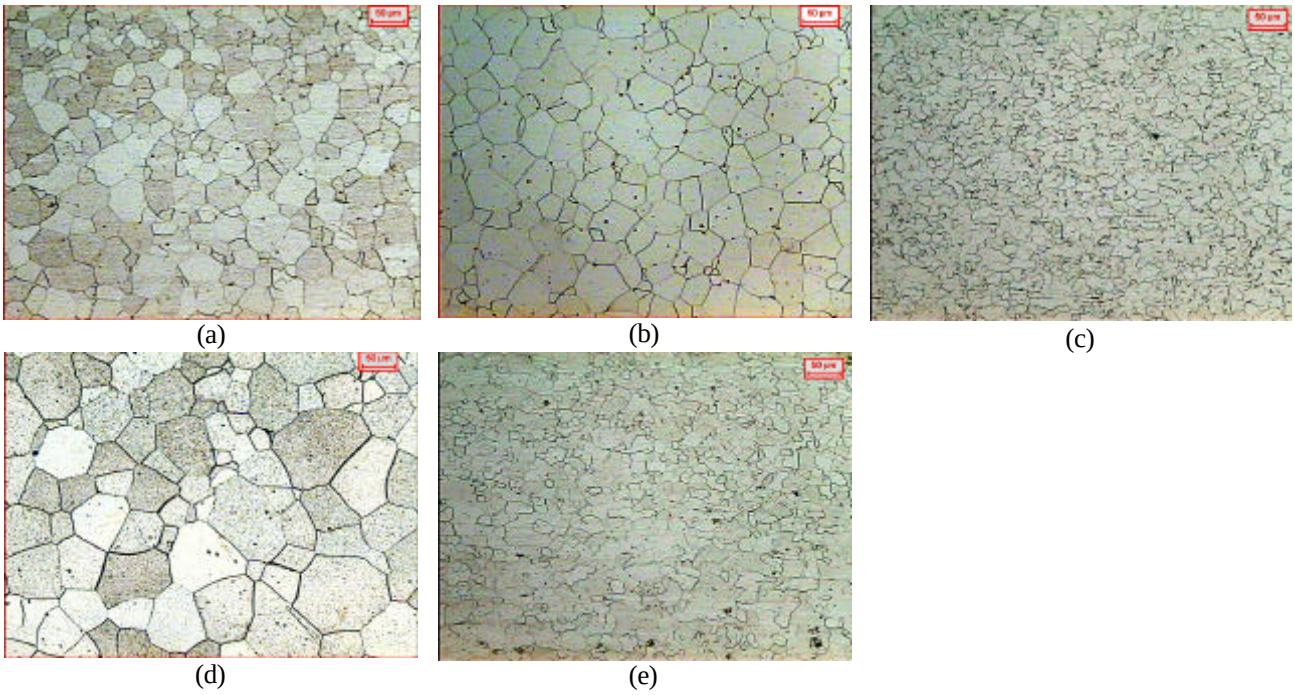

(a) (b) (c)

(d) (e)

Figure 3. Optical microstructure of the ferritic stainless steels, transversal direction, Villela's reagent. 200X.
(a) 409A; (b) 439A; (c) 430E; (d) 441A; (e) F17T.

Table 2. Measurement of grain size for ferritic stainless steels (μm).

P409A	P430E	P439A	P441A	F17T
30,5	14,5	49,4	64,3	16,5

We can see the smaller grain size of the 430E and F17T steels. In many ferritic stainless steels, because they comprise single-phase microstructures, grain growth is rapid. Due to the greater atomic mobility in ferritic structures, the ferritic chromium steels show more rapid grain growth and lower grain-coarsening temperatures than do the austenitic stainless steels. Ferritic steels start to coarsen rapidly from about 600°C, compared with about 900°C for austenitic steels (Pickering, 1983). The presence of Ti(CN) or Nb(CN) second-phase particles, however, retards grain growth and increases the grain-coarsening temperature. Surprisingly, the grain size of the 441A steel is large, even considering that this steel contains the greater content of Nb between the steels studied. This grain size difference can be explained by heat treatment during its production. The inclusions content in all the steels was fewer than generally expected for carbon steels.

3.2 Tensile tests

Stress-strain curves obtained from tensile tests for the materials in longitudinal direction are showed in Fig. 4. Typical mechanical properties (YS = yield stress; UTS = ultimate tensile stress; $\Delta L/L_o$ = elongation) are given in Tab. (3).

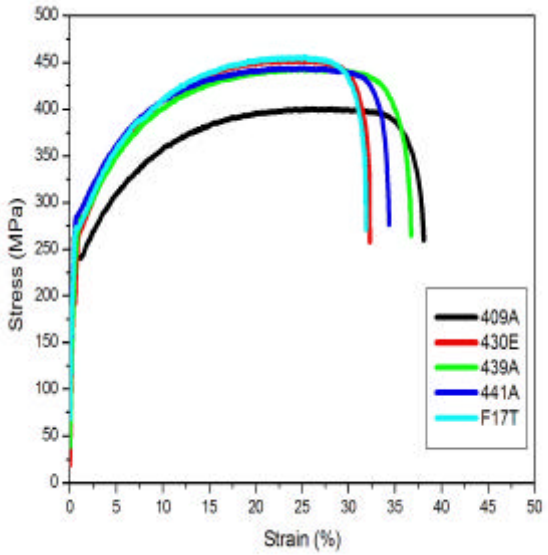

Figure 4. Stress-strain curves for the ferritic stainless steels. Longitudinal direction.

Table 3. Tensile mechanical properties of the ferritic stainless steels. Longitudinal direction.

Steel	YS (MPa)	UTS (MPa)	$\Delta L/L_o$ (%)
ACE P409A	240	401	38
ACE P439A	278	437	37
ACE P430E	259	449	32
ACE P441A	284	443	34
UGI F17T	275	453	32

We can see the different behavior of the steels and the better mechanical resistance of the 430E and F17T grades. Refinement of the ferrite grain size d increases the yield and tensile strengths according to the Hall-Petch relationship, i.e., the strength is a linear function of $d^{-1/2}$.

Solid solution hardening effects (substitutional solutes like Mn and interstitial solutes like C and N) and precipitation hardening effects (carbonitrides of Nb and Ti) are similar to those in low-carbon steels (Pickering, 1983). P409A grade presents more ductility and a little hardening because of its poor alloy content, mainly, chromium.

Fractographic analysis showed a transgranular and ductile fracture in all the steels, with a micromechanism of void nucleation, growth and coalescence, even considering the different mechanical behavior of the five steels. Figure 5(a,b,c,d,e) shows these results.

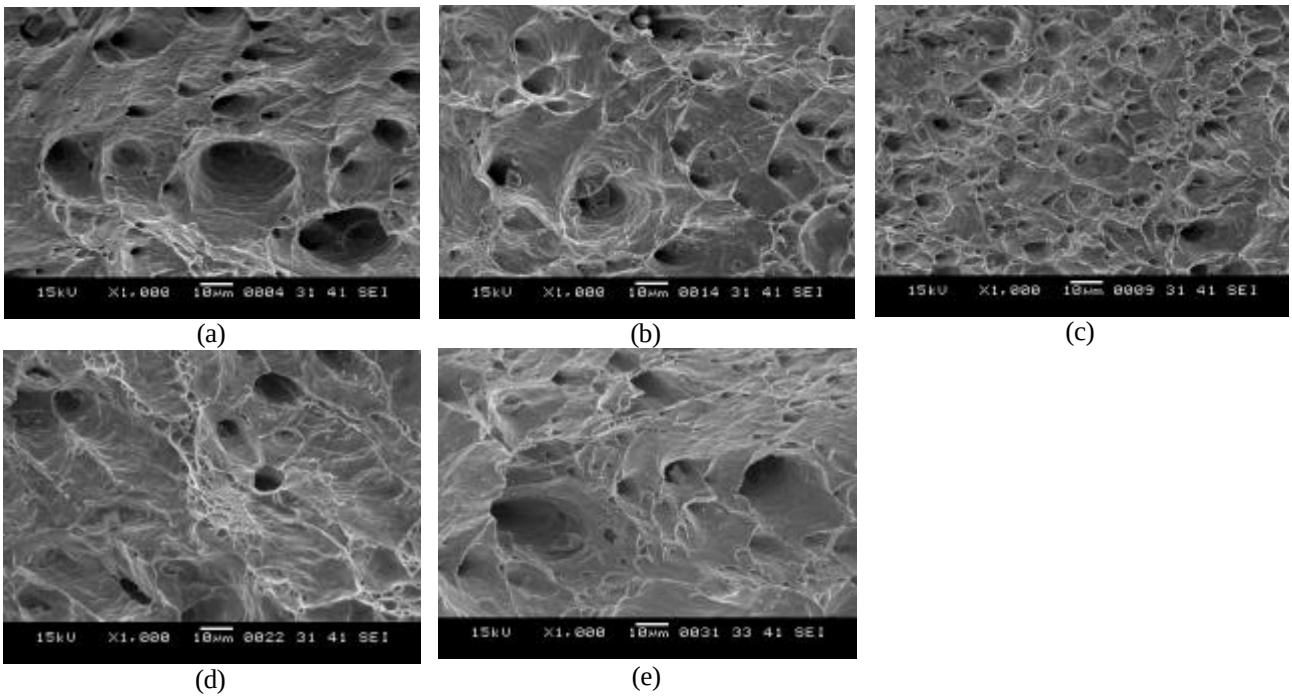

(a) (b) (c)

(d) (e)

Figure 5. SEM fractography of tensile surface from the ferritic stainless steels specimens, longitudinal direction, 1000X. (a) 409A; (b) 439A; (c) 430E; (d) 441A; (e) F17T.

3.3 Fatigue tests

Stress-life (S-N) results obtained from fatigue tests for the materials in longitudinal direction are showed in Fig. 6. The data points were fitted with a logarithmic function $log[N] = A - B\ log\ [S_{max} - C]$, where A, B and C are constants. For all specimens the scatter in the number of cycles to failure is relative small, due to the specimen geometry used and the inclusions content. The estimation of the fatigue limit FL based on 10^7 cycles, in terms of alternating fatigue strength, i.e., $[S_{max} - S_{min}]/2$ is presented in Tab. (4). This table repeats the YS and UTS limits presented in Tab. (2) for comparison, and shows the fatigue ratios FL/UTS and FL/YS.

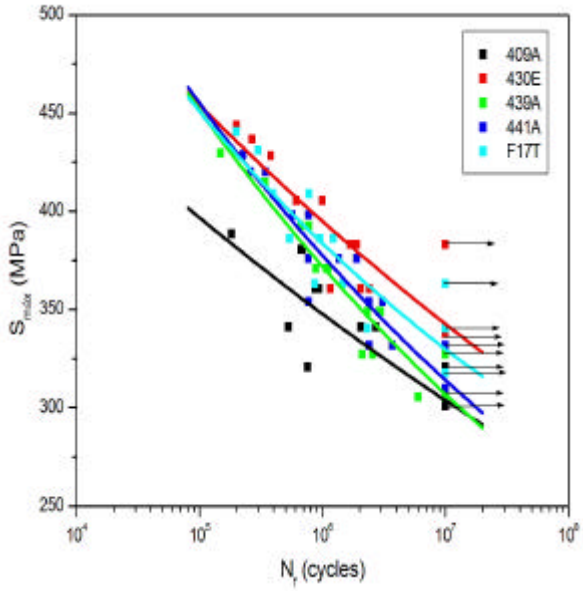

Figure 6. S-N data for the ferritic stainless steels. Longitudinal direction. Arrows denote no failure (three specimens).

Table 4. Estimation of the fatigue limit for the ferritic stainless steels. Longitudinal direction.

Steel	FL (MPa)	YS (MPa)	UTS (MPa)	FL/UTS	FL/YS
ACE P409A	137	240	401	0.34	0.57
ACE P439A	139	278	437	0.32	0.50
ACE P430E	155	259	449	0.35	0.59
ACE P441A	142	284	443	0.32	0.50
UGI F17T	149	275	453	0.33	0.54

An old idea is that the fatigue limit FL can be increased by raising the strength of a material, either by the chemical composition of the alloy, or by a heat treatment which increases the hardness (Hertzberg, 1989; Schijve, 2001). Results for different C-steels and low-alloy steels show that the fatigue ratio FL/UTS can vary between 0.30 and 0.60. Hardening effects present in all stainless steels of this research, like ferrite grain size, solid solution and precipitation, influenced the fatigue behavior of these steels, and furnished better results for the 430E steel.

It's interesting to note that it seems to be more logical to relate FL to YS. The tensile strength is depending on the strain hardening of the material after substantial plastic deformation has occurred. The yield stress is more characteristic for the small plastic strain behaviour. This is the reason that Tab. (4) shows the fatigue ratio FL/YS.

Fractographic analysis showed a similar aspect in all the steels, even considering the different mechanical behavior of the steels. During the period of fatigue life it's seen a flat fracture surface, indicating the absence of an appreciable amount of plastic deformation, The micromechanism of failure is divided in four parts: crack initiation at a corner or in the middle of the rectangular section, irregular crack growth by crystallographic facets, crack growth by striations and final ductile rupture. Figure 7(a,b,c,d) shows an example of these results, for the 441A steel, S_{max} = 80% UTS.

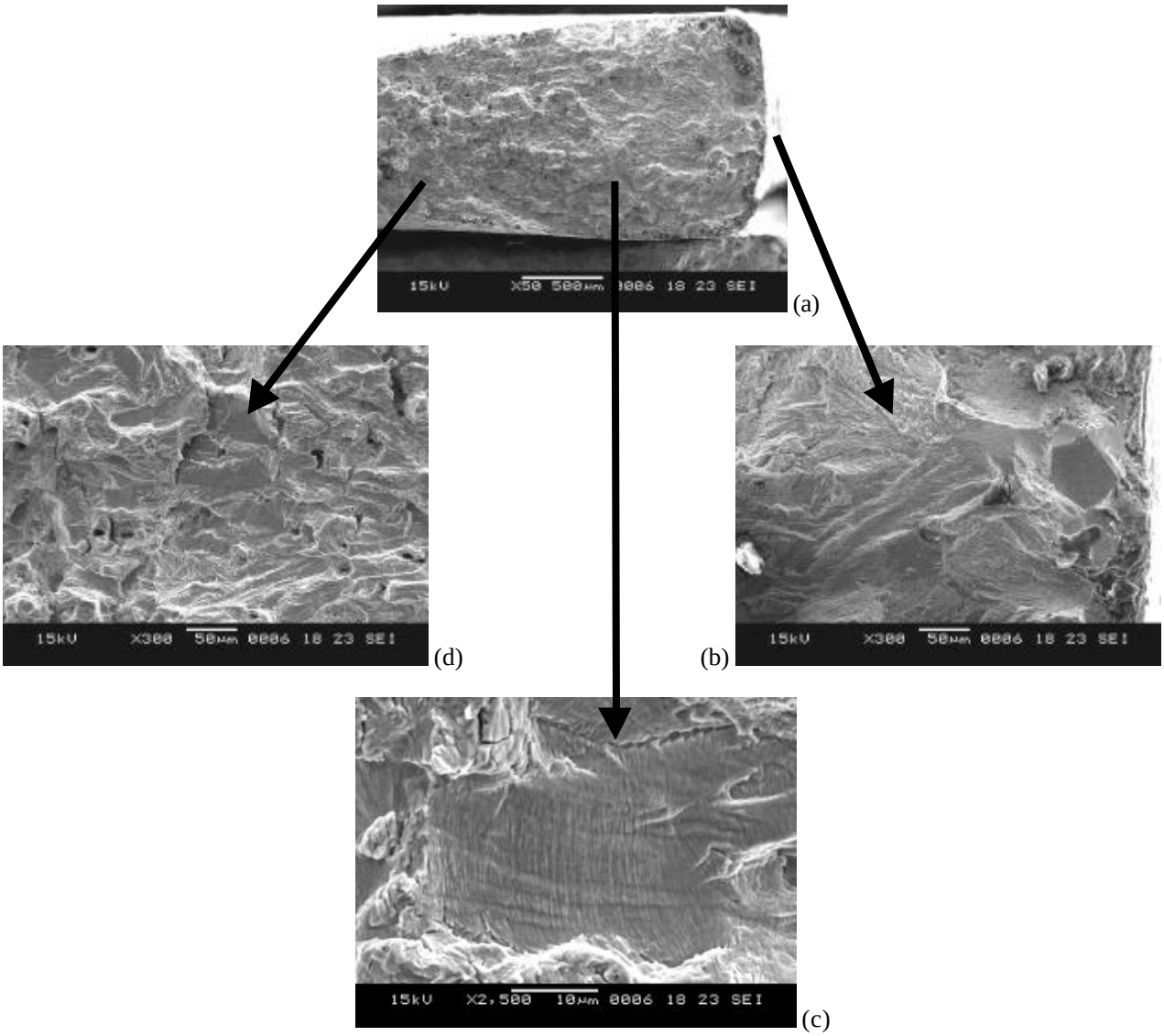

Figure 7. SEM fractography of fatigue surface from the 441A ferritic stainless steels, longitudinal direction. (a) general view, 50X; (b) crack origin and crack growth by facets, 300X; (c) crack growth by striations; (d) transition from fatigue to final ductile failure.

Due to the emission control for vehicles, the automotive industry has been forced to install exhaust systems with catalytic converters. The catalytic converter can and the manifold at the hot front are typical consumers of ferritic stainless steels (Heisterkamp and Carneiro, 2001). For this purpose at the hot part of the exhaust system, a ferritic stainless steel like the 441A is preferably alloyed with over-stoichiometric additions of Nb, because the Nb in solution forms a Laves phase, which improves the creep behavior, whereas the Nb precipitates give higher elevated temperature strength. On the other hand, if we intend to use the 441A stainless steel in the cold part of the exhaust system (where

fatigue is more pronounced than creep and hot degradation), we must control the ferrite grain size to give smaller grains than we obtained in this research.

4. Conclusions

Tensile strength and fatigue strength of the five ferritic stainless steels studied in this research were directly related to ferrite grain size and the presence of solid solution elements and precipitates. In ambient temperature the resistance of the 430E steel stabilized with Nb was superior to the other steels. This steel had the better combination of small grain size, substitutional and interstitial solid solution elements and carbonitrides precipitates.

5. Acknowledgements

The authors would like to thank ACESITA S.A, UGINE &ALZ and CBMM S.A. for ferritic stainless steels donations and technical support.

6. References

Bergengren, Y., Larsson, M. and Melander, A., 1995, "Fatigue properties of stainless steels in air at room temperature", Materials Science and Technology, Vol. 11, pp. 1275-1279.
Douhett, J. A., 1995, "Designing stainless exhaust systems", Automotive Engineering, November, pp. 45-49.
Gordon, W. and Bennekom A., 1996, "Review of stabilization of ferritic stainless steels", Materials Science and Technology, Vol.12, pp. 126-131.
Heistercamp, F. and Carneiro, T., 2001, "Proceedings of the International Symposium Niobium 2001", TMS, pp. 1109-1159.
Hertzberg, R.W., 1989, "Deformation and Fracture Mechanics of Engineering Materials", John Wiley & Sons, pp. 476-482.
Hiramatsu, N., 2001, "Niobium in ferritic and martensitic stainless steels", Proceedings of the International Symposium Niobium 2001, TMS, pp. 961-974.
Kawasaki Steel, 2001, "An introduction to iron and steel processing, www.kawasaki-steel.co.jp
Keown, S.R. and Pickering, F.B., 1984, "Niobium in stainless steel", Proceedings of the International Symposium Niobium 1981, TMS, pp. 1113-1142.
Llewellyn, D.T., 1994, "Steels – Metallurgy and Applications", Butterworth-Heinemann Ltd., pp. 295-297.
Pickering, F.B., 1979, "The physical metallurgy of 12% chromium steels", The Metallurgical Evolution of Stainless Steels, ASM, pp. 1-42.
Pickering, F.B., 1983, "Physical Metallurgy and the Design of Steels", Applied Science Publishers, pp. 201-225.
Schijve, J., 2001, "Fatigue of Structures and Materials", Kluwer Academic Publishers, pp. 122-124.
Schmitt, J.H., 2002, "Some examples of stainless steel use in the automotive industry", Key Engineering Materials, Vols. 230-232, pp. 17-22.

7. Responsibility notice

The authors are the only responsible for the printed material included in this paper.